

**Cell Reports, Volume 43**

**Supplemental information**

**Ligand-induced segregation from large  
cell-surface phosphatases is a critical  
step in  $\gamma\delta$  TCR triggering**

**Fenglei Li, Sobhan Roy, Jacob Niculcea, Keith Gould, Erin J. Adams, P. Anton van der Merwe, and Kaushik Choudhuri**

**Figure S1.**

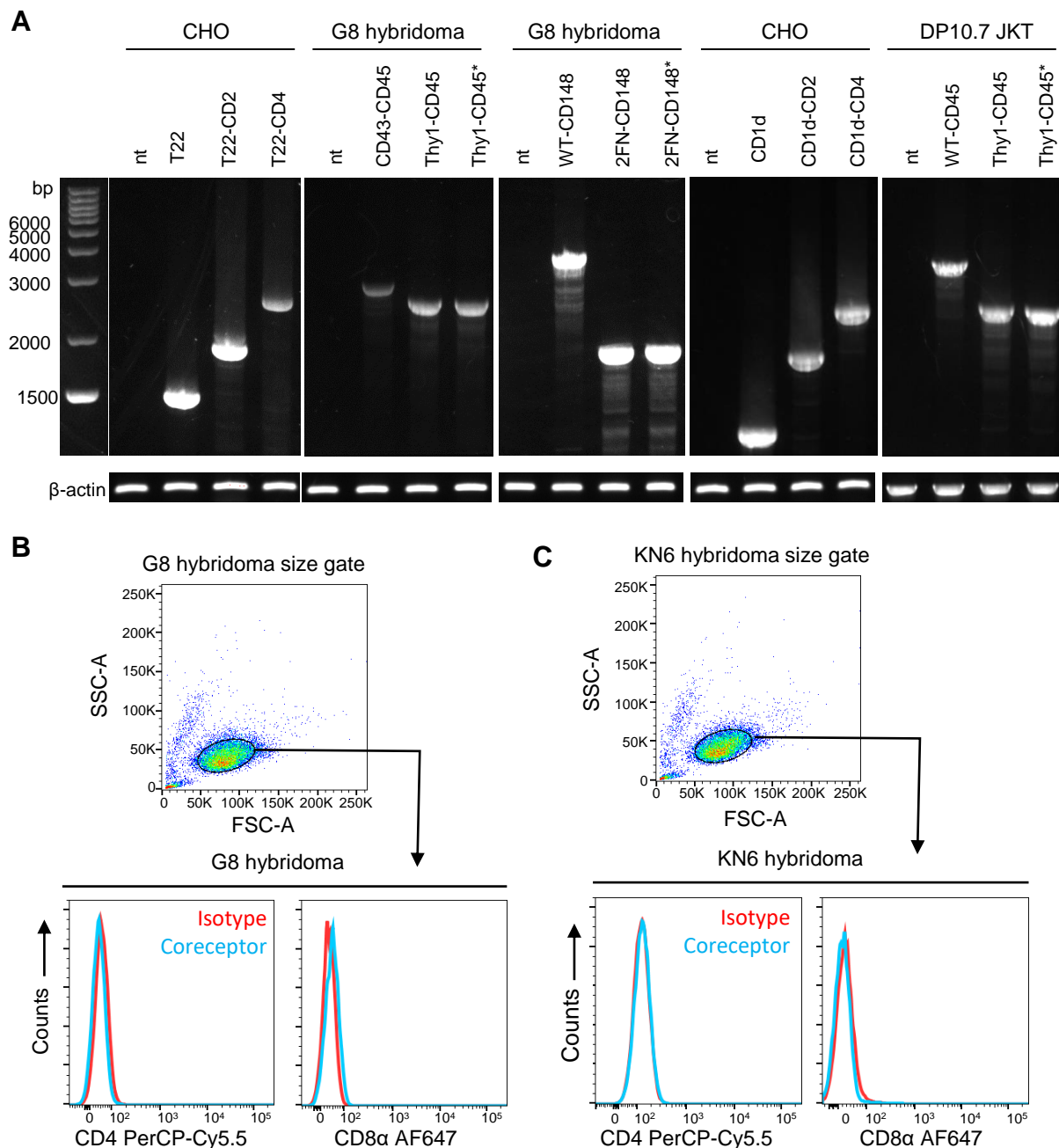


**Figure S1. Characterization of CHO cell transductants and T cell hybridomas (related to expression constructs and cell lines in Figures 1, 5 and 7).**

(A) RT-PCR of total RNA extracted from the indicated cell lines stably transduced with the indicated constructs. RT-PCR reactions were performed using the primers listed in Supplementary Table 2.

(B), (C) Gating strategy and histogram overlays of surface expression of co-receptors CD4 and CD8 (cyan lines) in (B) G8, and (C) KN6, T cell hybridomas as measured by flow-cytometry.

**Figure S2.**

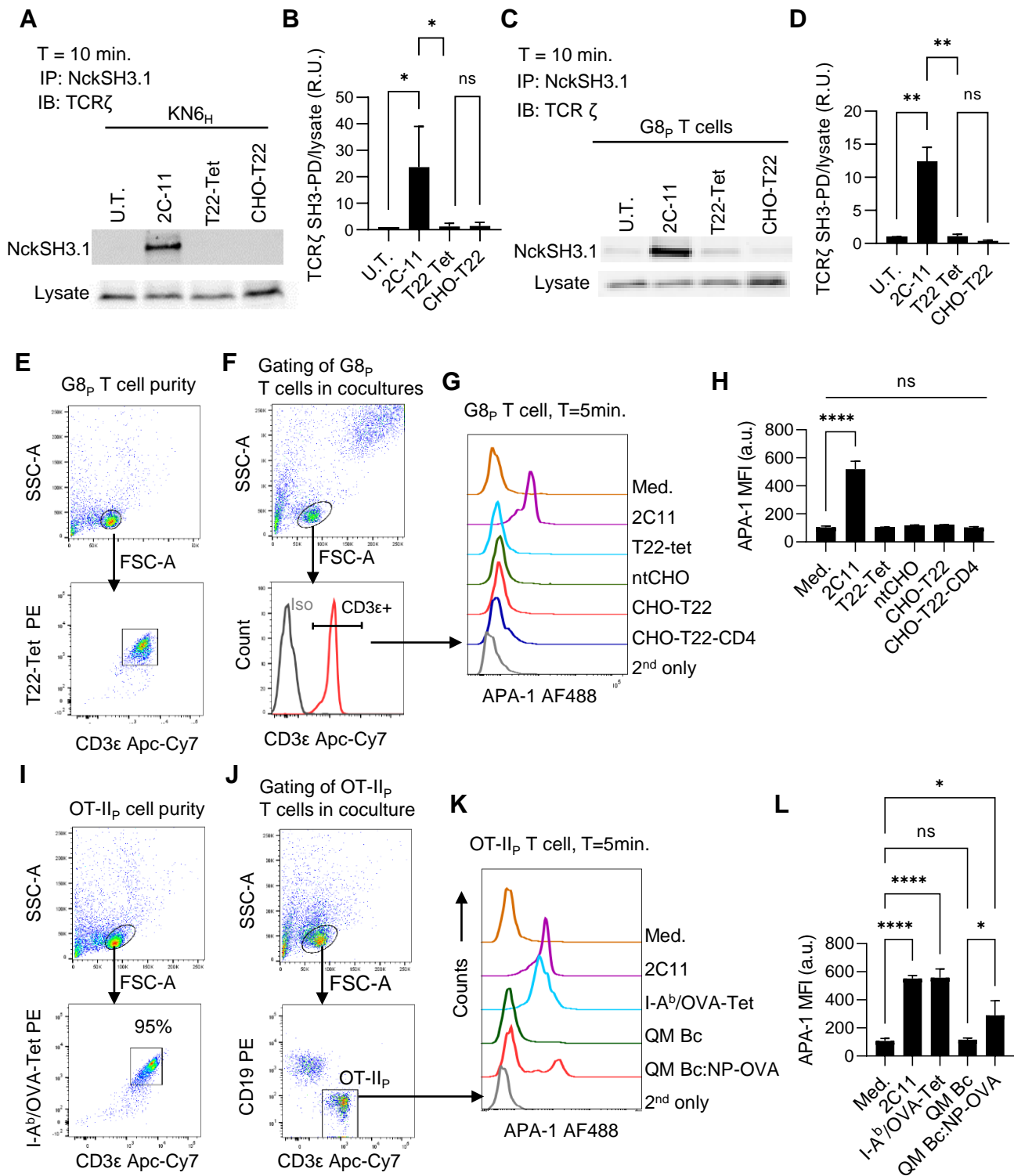


**Figure S2.  $\gamma\delta$  TCR triggering does not require conformational changes typical of  $\alpha\beta$  TCRs (related to Figures 1 and 2, figure legend on following page).**

**Figure S2. KN6 and G8  $\gamma\delta$  TCR triggering does not require conformational changes typical of  $\alpha\beta$  TCRs (related to Figures 1 and 2).**

(A) Representative immunoblot of TCR $\zeta$  in Nck SH3.1 pulldowns from KN6 T cell hybridomas (KN6<sub>H</sub>) following 10 min incubation with anti-CD3 $\epsilon$  antibody 2C11, T22 tetramer (T22 Tet), or CHO cells expressing T22 SCD. TCR $\zeta$  blots of input lysates is shown as a loading control.

(B) Quantitation of blots as in (A). Data are presented as normalized ratios of TCR $\zeta$  density in Nck SH3.1 pulldowns (TCR $\zeta$  SH3-PD) over TCR $\zeta$  density in corresponding input lysates.  $n = 3$ , data are mean  $\pm$  SD.

(C) Representative immunoblot of TCR $\zeta$  in Nck SH3.1 pulldowns from primary G8 T cell hybridomas (G8<sub>p</sub>) following 10 min incubation with anti-CD3 $\epsilon$  antibody 2C11, T22 tetramer, or CHO cells expressing T22 SCD. TCR $\zeta$  blots of input lysates is shown as a loading control.

(D) Quantitation of blots as in (C). Data are presented as normalized ratios of TCR $\zeta$  in Nck SH3.1 pulldown (TCR $\zeta$  SH3-PD) over TCR $\zeta$  in corresponding input lysates.  $n = 2$ , data are mean  $\pm$  SD.

(E) Flow cytometry dot plots showing size gate and purity of primary G8 T cells (G8<sub>p</sub>) stained with fluorescently labelled cognate T22 tetramer (T22-Tet) and anti-CD3 $\epsilon$  antibody.

(F) Gating of G8<sub>p</sub> T cells in cocultures with CHO cell transductants.

(G) Histogram cascade plots of G8<sub>p</sub> T cells gated as in (F) stained with fluorescently labelled conformation-sensitive CD3 $\epsilon$  antibody APA1/1, after incubation for 5min at 37°C in medium alone (Med.), or with 2C11 antibody, T22-Tet, non-transduced CHO cells (ntCHO), or with the indicated CHO cell transductants.

(H) Quantitation of APA1/1 staining intensity (MFI) of G8<sub>p</sub> T cells as in (G).  $n = 3$ , data are mean  $\pm$  SD. a.u, arbitrary units.

(I) Flow cytometry dot plots showing size gate and purity of primary OTII  $\alpha\beta$  T cells (OT-II<sub>p</sub>) stained with fluorescently labelled cognate I-A<sup>b</sup>/OVA<sup>323-339</sup> tetramer (I-A<sup>b</sup>/OVA-Tet) and anti-CD3 $\epsilon$  antibody.

(J) Gating of OT-II<sub>p</sub> T cells in cocultures with QM B cells (CD19<sup>+</sup>).

(K) Histogram cascade plots of OT-II<sub>p</sub> T cells gated as in (J) stained with with fluorescently labelled conformation-sensitive CD3 $\epsilon$  antibody APA1/1, after incubation for 5min at 37°C in medium alone (Med.), or with 2C11 antibody, I-A<sup>b</sup>/OVA-Tet, unloaded QM B cells (QM Bc), or with ovalbumin-loaded QM B cells (QM Bc:NP-OVA).

(L) Quantitation of APA1/1 staining intensity (MFI) of OT-II<sub>p</sub> T cells as in (K).  $n = 3$ , data are mean  $\pm$  SD. a.u, arbitrary units.

Means were compared by 1-way ANOVA corrected for all pairwise comparisons. \*,  $P < 0.05$ ; \*\*,  $P < 0.001$ ; \*\*\*,  $P < 0.0001$ ; ns, not significant ( $P > 0.05$ ).

**Figure S3.**

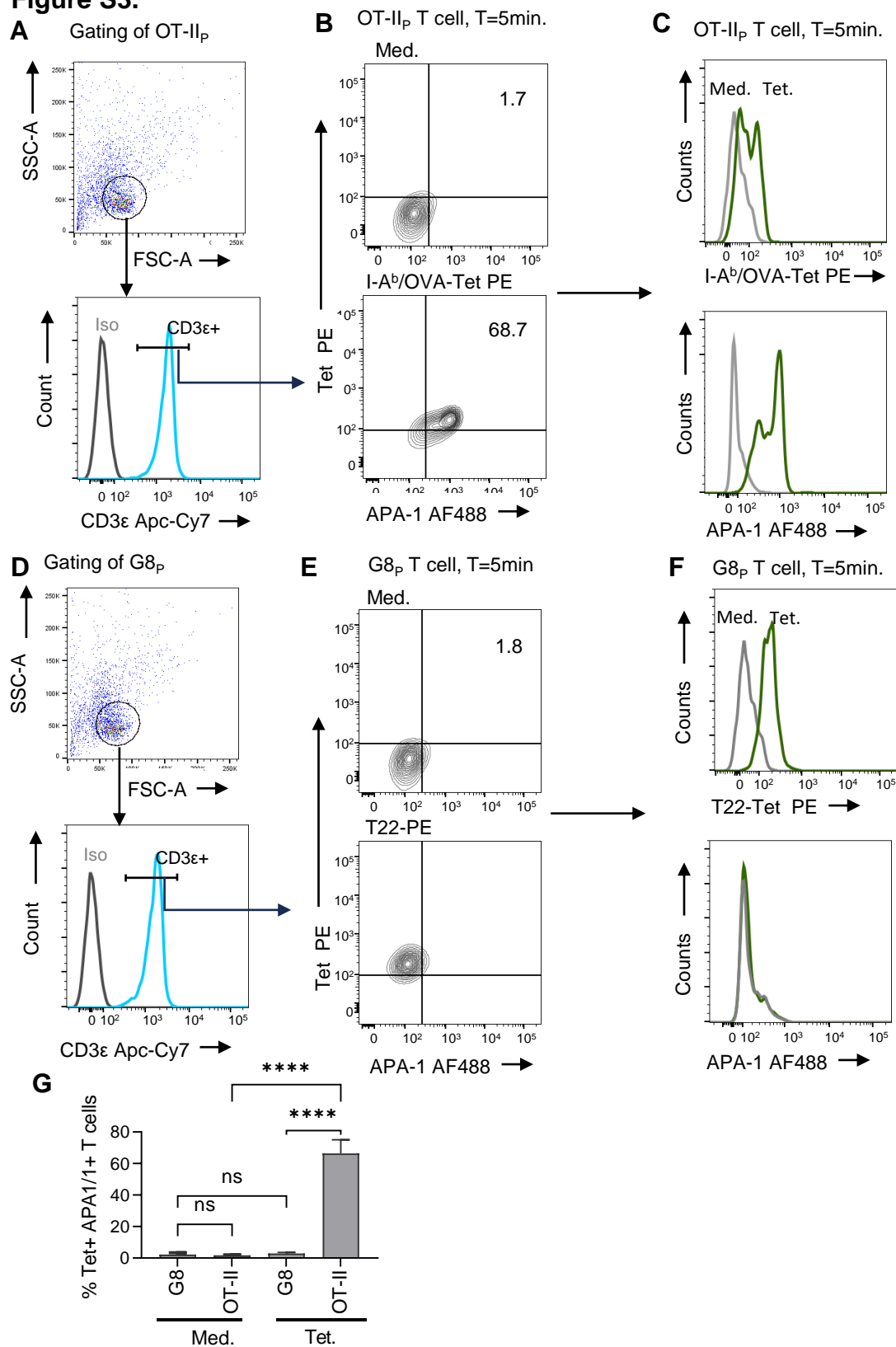


**Figure S3. Absence of T22 tetramer-induced conformational change in G8 TCRs is not due to tetramer unbinding.** (related to Figures 1 and 2, figure legend on following page).

**Figure S3. Absence of T22 tetramer-induced conformational change in G8 TCRs is not due to tetramer unbinding.**

(A) OT-II<sub>p</sub> and (D) G8<sub>p</sub> T cells were incubated with the indicated fluorescently labeled tetramers (Tet) or medium (Med) alone for 5 min, following washing, were fixed, permeabilized and stained with fluorescently-labeled conformation sensitive antibody specific for the cytoplasmic portion of CD3ε (APA1/1) and CD3ε ectodomain-specific antibody for gating. Shown are scatter plots indicating the live cell size gate and TCR+ serial gates.

(B,E) Contour plots of TCR-gated OT-II<sub>p</sub> (B) and G8<sub>p</sub> (E) T cells showing APA1/1 staining and levels of cell-bound cognate tetramers.

(C,F) Histogram overlays of TCR-gated OT-II<sub>p</sub> (C) and G8<sub>p</sub> (F) T cells showing APA1/1 staining and levels of cognate tetramer binding.

(G) Quantitation of Tetramer+ APA1/1+ cells. Means were compared by 1-way ANOVA corrected for all pairwise comparisons. \*\*\*\*,  $P < 0.0001$ ; ns, not significant ( $P > 0.05$ ).

**Figure S4.**

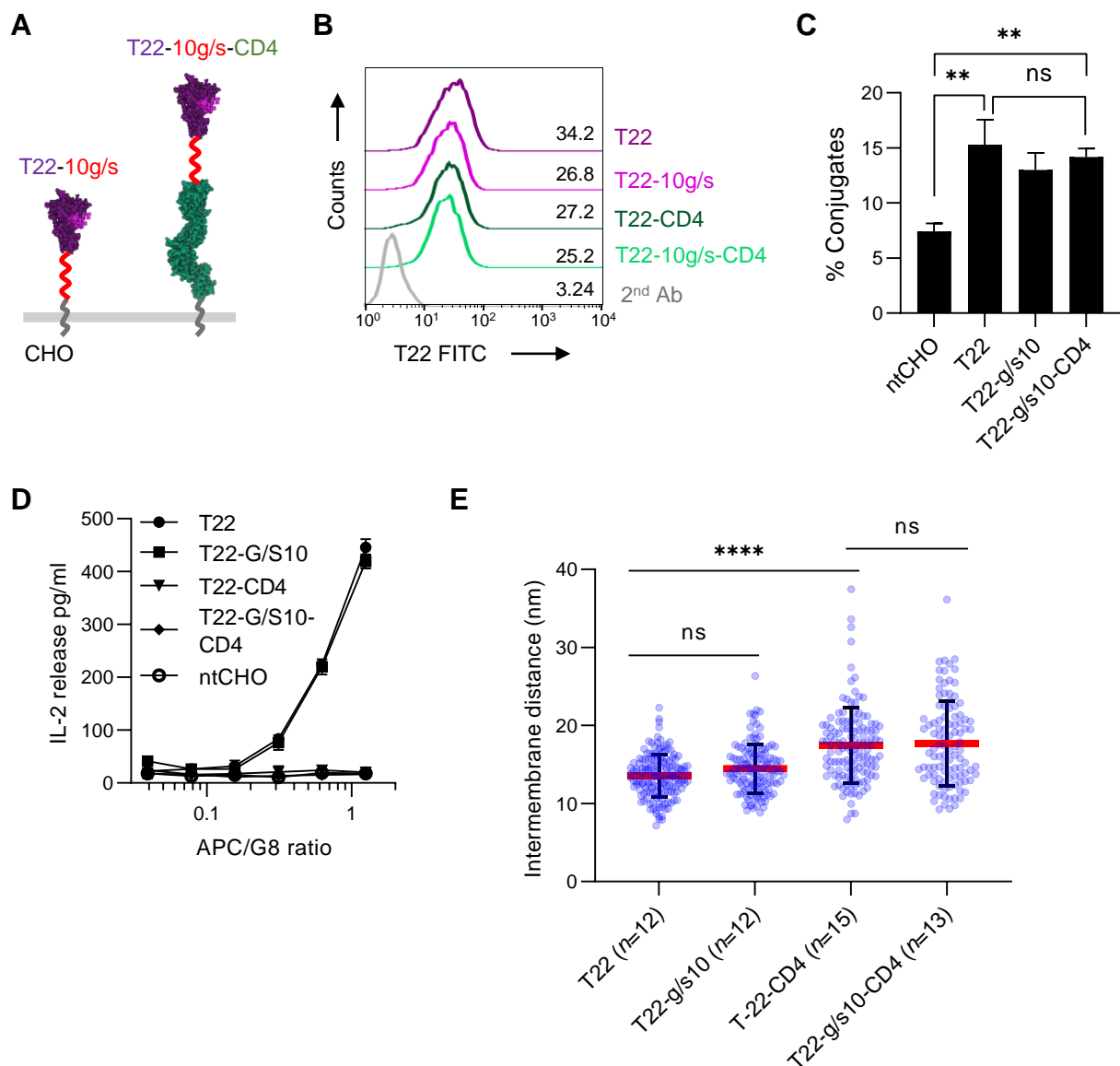


**Figure S4. G8<sub>H</sub> T cell activation and intermembrane distance at synapses is unaffected by increased T22 flexibility (related to Figures 1 and 3, figure legend on following page)**

**Figure S4. G8<sub>H</sub> T cell activation and intermembrane distance at G8 synapses is unaffected by increased T22 flexibility (related to Figures 1 and 3).**

**(A)** Cartoon schematic of T22 and CD4-elongated T22 in which the 5 residue glycine/serine (g/s) linkers (grey) at the T22 C-terminus were replaced with 10 residue glycine/serine linkers (red) to increase flexibility of chimeric constructs.

**(B)** Histogram cascade plots of CHO cell surface expression of the indicated T22 constructs as measured by flow-cytometry. Constructs were stably expressed in CHO cells and sorted for comparable expression.

**(C)** Cell-cell adhesion as measured by conjugate formation between G8 T cell hybridomas and CHO cells expressing indicated T22 constructs. Results are representative of 3 independent experiments. Data are mean  $\pm$  SD.

**(D)** Activation of G8  $\gamma\delta$  T cell hybridomas in response to original and flexible forms of T22, as measured by IL-2 release.  $10^4$  G8  $\gamma\delta$  T cell hybridomas were cocultured with increasing numbers of T22-expressing CHO cells for 24 hrs (expressed as APC/G8 cell ratio), and IL-2 release in culture supernatants measured by ELISA. Results are representative of 3 independent experiments. Data are mean  $\pm$  SD.

**(E)** Intermembrane distances measured at synaptic contacts between G8  $\gamma\delta$  T cell hybridomas and CHO cells expressing original and flexible versions of T22 and CD4-elongated T22. Data points are individual intermembrane distance measurements in each group. The number of conjugates sampled ( $n$ ) is indicated for each group. Red line indicate mean and error bars are  $\pm$ SD.

Means were compared by 1-way ANOVA corrected for all pairwise comparisons. \*\*,  $P < 0.001$ ; \*\*\*,  $P < 0.0001$ ; ns, not significant ( $P > 0.05$ ).



**Figure S5.**

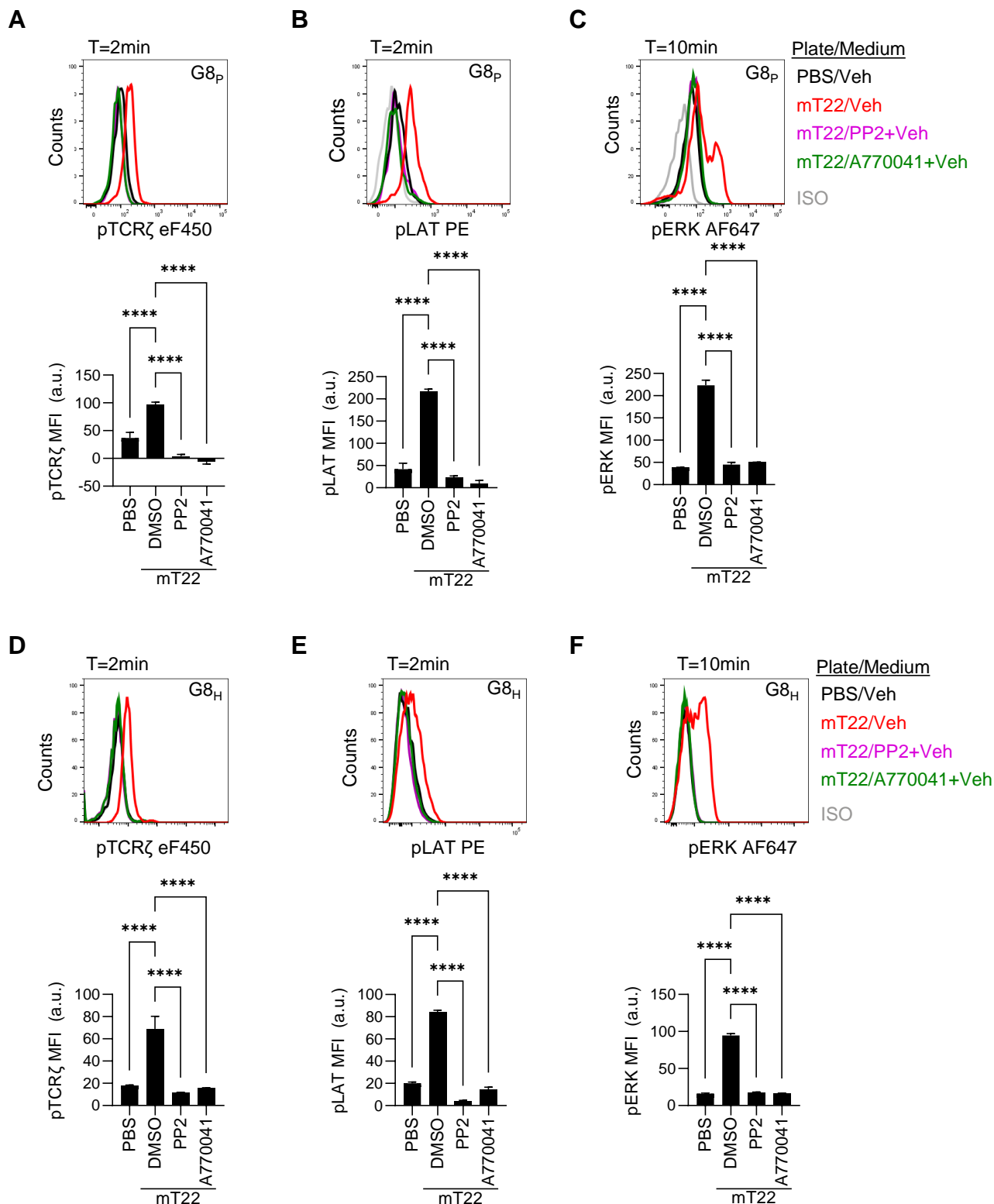


**Figure S5. Lck activity is critical for T22-mediated G8 TCR phosphorylation and downstream signal transduction. (related to Figures 1 and 2, figure legend on following page).**

**Figure S5. Lck activity is critical for T22-mediated G8 TCR phosphorylation and downstream signal transduction. (related to Figures 1 and 2).**

**(A) Top panel,** Flow cytometry histogram overlay of pCD3 $\zeta$  antibody staining of primary G8 T cells (G8<sub>p</sub>), pretreated with the indicated inhibitors, or with DMSO vehicle alone (Veh), and incubated for 2 minute at 37°C on plate-adsorbed recombinant T22 monomers (mT22), or in uncoated wells (PBS). ISO, Isotype control antibody staining. **Bottom panel,** Quantitation of pCD3 $\zeta$  antibody staining as in *Top Panel*.

**(B) Top panel,** Histogram overlay of pLAT antibody staining in primary G8 T cells (G8<sub>p</sub>) treated as in (A). **Bottom panel,** Quantitation of pLAT antibody staining as in (A, *Bottom Panel*).

**(C) Top panel,** Histogram overlay of pERK antibody staining in primary G8 T cells (G8<sub>p</sub>) pretreated as in (A), and incubated for 10 min at 37°C on plate-adsorbed recombinant T22 monomers (mT22), or in uncoated wells (PBS). **Bottom panel,** Quantitation of pERK antibody staining as in (A).

**(D) Top panel,** Histogram overlay of pCD3 $\zeta$  antibody staining in G8 T cell hybridomas (G8<sub>H</sub>), treated as in (A). **Bottom panel,** Quantitation of pCD3 $\zeta$  antibody staining as in (A).

**(E) Top panel,** Histogram overlay of pLAT antibody staining in G8<sub>H</sub> T cells treated as in (A). **Bottom panel,** Quantitation of pLAT antibody staining as in (A, *Bottom Panel*).

**(F) Top panel,** Histogram overlay of pERK antibody staining in G8<sub>H</sub> T cells pretreated as in (A), and incubated for 10 min at 37°C on plate-adsorbed recombinant T22 monomers (mT22), or in uncoated wells (PBS). **Bottom panel,** Quantitation of pERK antibody staining as in (A).

Data are MFI after background subtraction of mean ISO values, and results are representative of 3 independent experiments. Mean  $\pm$  SD is shown. Means were compared by 1-way ANOVA and corrected for all pairwise comparisons. \*\*\*\*\*,  $P < 0.0001$ .

**Figure S6.**

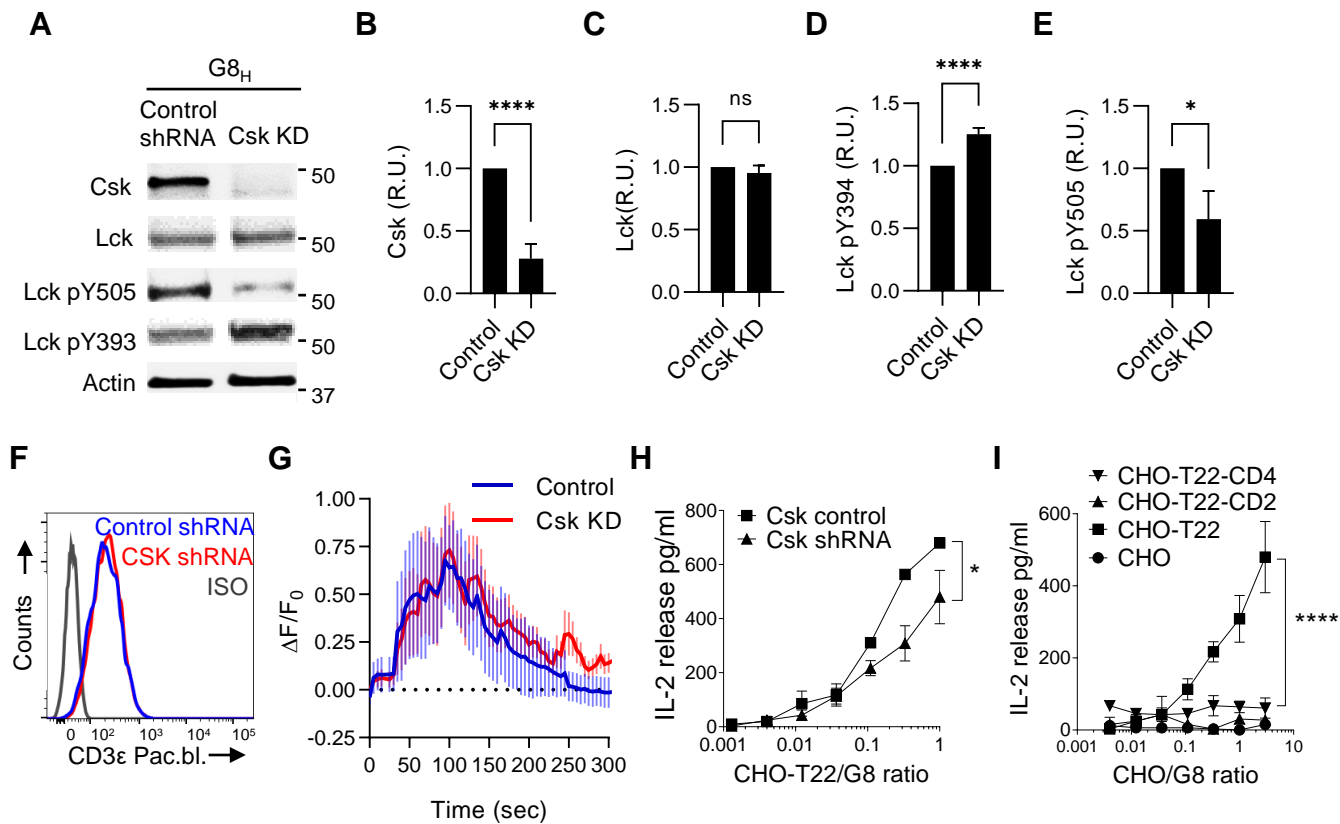


**Figure S6. Suppression of Csk expression increases active Lck levels but fails to rescue TCR triggering in response to elongated T22 (related to Figure 1, figure legend on following page).**

**Figure S6. Suppression of Csk expression increases active Lck levels but fails to rescue TCR triggering in response to elongated T22.**

**(A)** Immunoblots of resting G8<sub>H</sub> T cell lysates that were stably transduced with Csk-targeting or non-targeting control shRNA. Cell lysates were analyzed using antibodies for Csk, and antibodies specific for the tyrosine phosphorylated positive (Y393) and negative (Y505) regulatory sites of Lck. A representative blot from 3-5 independent experiments is shown.

**(B)-(E)** Quantitation of the indicated phosphorylated proteins from immunoblots as in **(A)**. B:  $n = 4$ , C, E:  $n = 5$ , D:  $n = 3$ .

**(F)** Cell-surface TCR expression levels of G8<sub>H</sub> T cells transduced with the indicated shRNA expression vectors shRNA. Cells were labeled with an anti-CD3 $\epsilon$  antibody and analyzed by flow-cytometry.

**(G)** Analysis of Ca<sup>2+</sup> signaling in live G8<sub>H</sub> T cells transduced with Csk targeting (Csk KD) or non-targeting (Control) shRNA following contact with planar lipid bilayers containing 100 molecules/ $\mu\text{m}^2$  T22 and 350 molecules/ $\mu\text{m}^2$  ICAM-1. T cells were loaded with Fluo-4 and Ca<sup>2+</sup> flux imaged by epifluorescence microscopy following contact with supported lipid bilayers (T=0). Plots represent (mean fluorescence - fluorescence at T=0)/(fluorescence at T=0)  $\pm$  SEM. Results are pooled from 2 independent experiments.

**(H)** Activation of G8<sub>H</sub> T cells stably transduced with Csk-targeting or control shRNA, as measured by IL-2 release after 24hrs co-culture with T22-expressing CHO cells. Results are representative of 3 independent experiments.

**(I)** IL-2 release in response to Increasing numbers of CHO cells expressing T22 and elongated forms of T22 (expressed as CHO/G8 ratio) by 10<sup>4</sup> G8<sub>H</sub> T cells expressing Csk-targeting shRNA. Results are representative of 3 independent experiments.

Mean  $\pm$  SD is shown. Means were compared by *t*-test. \*,  $P < 0.05$ ; \*\*\*\*,  $P < 0.0001$ . In **(H)** and **(I)** data means at G8/CHO ratio=1 are tested for the indicated comparisons.

**Figure S7.**

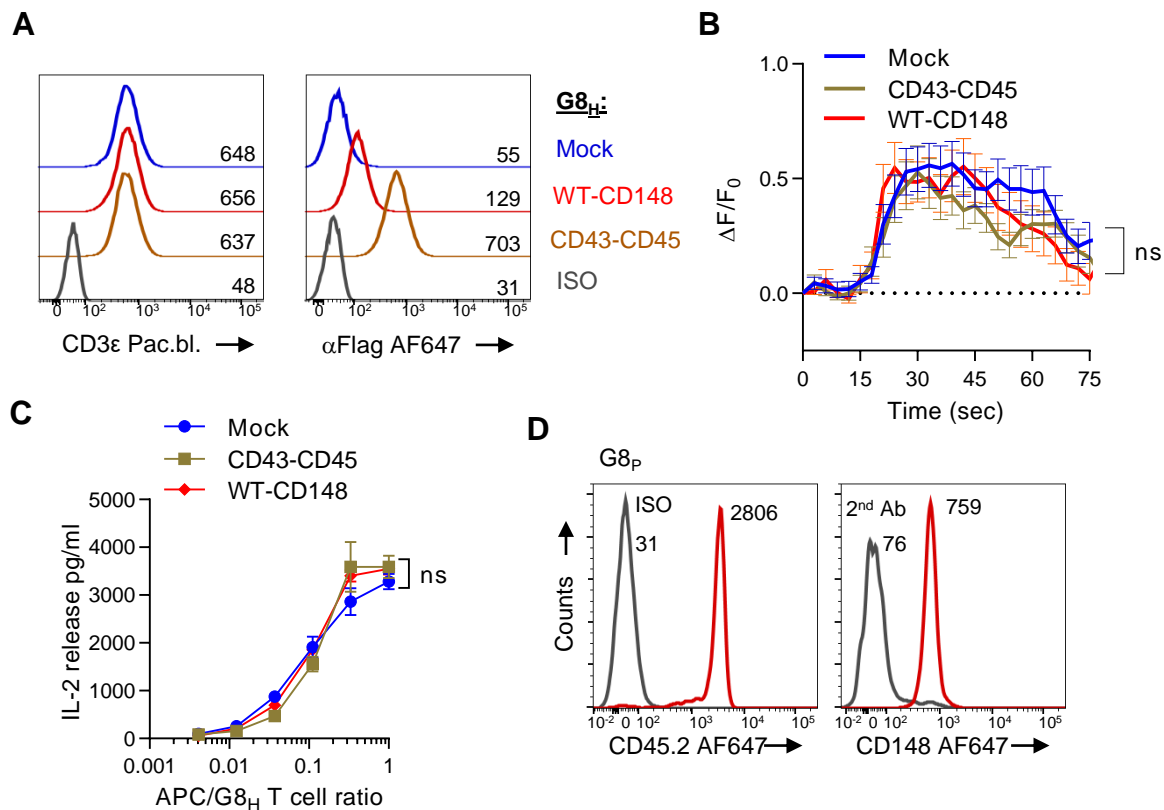


**Figure S7. Phenotype and function of lentivirally transduced G8<sub>H</sub> T cells. Related to Figure 5.**

(A) Cascade plots of surface expression levels of TCR and the indicated CD45/148 constructs, including an empty expression construct for mock transduction, following lentiviral transduction of G8<sub>H</sub> T cells. Flag-tagged constructs and surface TCR were detected by immunostaining and flow-cytometry.

(B) Analysis of Ca<sup>2+</sup> signaling in live G8<sub>H</sub> T cells, transduced with the indicated expression constructs, following contact with planar lipid bilayers containing 100 molecules/μm<sup>2</sup> T22 and 350 molecules/μm<sup>2</sup> ICAM-1. T cells were loaded with Fluo-4 and Ca<sup>2+</sup> flux imaged by epifluorescence microscopy following contact with supported lipid bilayers (T=0). Plots represent (mean fluorescence - fluorescence at T=0)/(fluorescence at T=0) ± SEM. Results are pooled from 3 independent experiments.

(C) Activation of the indicated G8<sub>H</sub> T cell transductants as measured by IL-2 release after 24hrs co-culture with T22-expressing CHO cells. Results are expressed as a ratio of increasing numbers CHO cells expressing T22 incubated with 10<sup>4</sup> G8<sub>H</sub> T cell transductants for 24hrs. Results are representative of 3 independent experiments.

(D) Flow-cytometry histograms showing surface expression levels of CD45 and CD148 on primary G8 (G8<sub>p</sub>) T cells. ISO, isotype control antibody.

**Figure S8.**

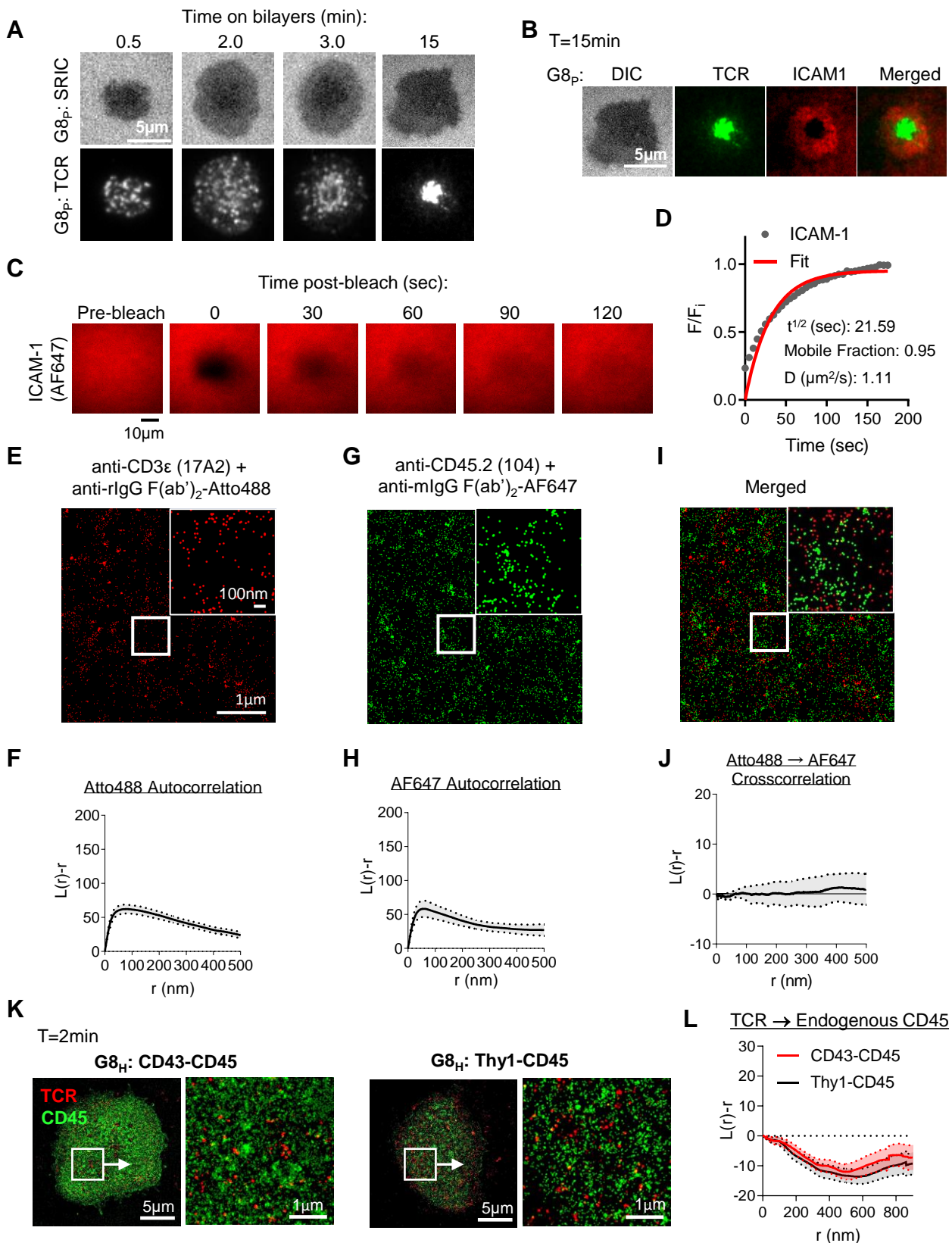


**Figure S8. Validation of imaging conditions and cell sample controls for TIRFM/dSTORM imaging of  $\gamma\delta$  T cell synapses on SLB (related to Figures 6 and 7, figure legend on following page).**

**Figure S8. Validation of imaging conditions and cell sample controls for TIRFM/dSTORM imaging of  $\gamma\delta$  T cell synapses on SLB (related to Figures 6 and 7).**

**(A)** Representative TIRFM images of G8<sub>p</sub> T cells forming synapses on SLB containing 100 molecules/ $\mu\text{m}^2$  T22 and 350 molecules/ $\mu\text{m}^2$  ICAM-1 at the indicated timepoints. T cells were incubated on bilayers for indicated times at 37°C. cells were then fixed,, permeabilized and labelled with an anti-CD3 $\epsilon$  antibody and a fluorescently-labeled 2<sup>nd</sup> antibody.

**(B)** Representative image of a G8<sub>p</sub> T cell forming a mature immunological synapse after 15 minutes interaction with SLB containing T22 and ICAM-1-AF647, and processed as in A.

**(C)** Time series of fluorescence recovery after photobleaching of AF647-labeled ICAM-His10 attached to SLB at 350 mol/ $\mu\text{m}^2$ . A prebleach image was taken prior to photobleaching of a 15 $\mu\text{m}$  diameter ROI using 633nm laser irradiation.

**(D)** The ratio of post-bleach fluorescence intensity captured at 5sec intervals ( $F_i$ ) over the pre-bleach fluorescence intensity ( $F_0$ ) was plotted over time to fit with one phase exponential function for extraction of recovery half-time  $t^{1/2}$ , diffusion coefficient  $D$ , and mobile fraction parameters.

**(E)** dSTORM Gaussian filtered localization image of rat anti-mCD3 $\epsilon$  mAb 17A2 adsorbed onto a PLL-coated coverslip. Indicated primary antibodies were adsorbed on PLL coverslip for 1hr at RT, fixed with 3% PFA for 45mins, quenched with 100mM glycine for 1hr, blocked with 5% BSA for 1hr, and stained with indicated 2nd antibody for 1hr (f/p ~ 2). Inset shows unfiltered localizations in white boxed region.

**(F)** Ripley's H-function autocorrelation of the Atto488 label.

**(G)** dSTORM localization image of the anti-CD45.2 mAb 104 labelled with a polyclonal anti-mIgG (H+L chain) F(ab')<sub>2</sub>-AF647 secondary antibody (f/p ~2).

**(H)** Autocorrelation of the AF647 label.

**(I)** Merged image of Atto488 and AF647 localizations.

**(J)** Ripley's H-function cross-correlation of Atto488 and AF647 labels. Negative values represent dispersion (segregation) and positive values represent clustering. Shaded region within dotted lines demarcate 95% confidence intervals.

**(K) Left panels,** Representative Gaussian-filtered images of endogenous TCR and CD45 localizations at synapses formed by G8 hybridoma (G8<sub>H</sub>) transduced with the indicated Flag-tagged CD45 chimeras (not detected). **Right panels,** High magnification Gaussian-filtered images of white boxed region in *left panels*.

**(L)** Cross-correlation of endogenous TCR and CD45 localizations. Graphs represent mean  $\pm$  SEM. CD43-CD45 transduced G8 hybridomas:  $n=39$  ROIs (pooled from 10 synapses); Thy1-CD45 transduced G8 hybridomas:  $n= 30$  ROIs (pooled from 11 synapses). Synapses were randomly chosen from pooled images from 3 independent experiments.

**Figure S9.**

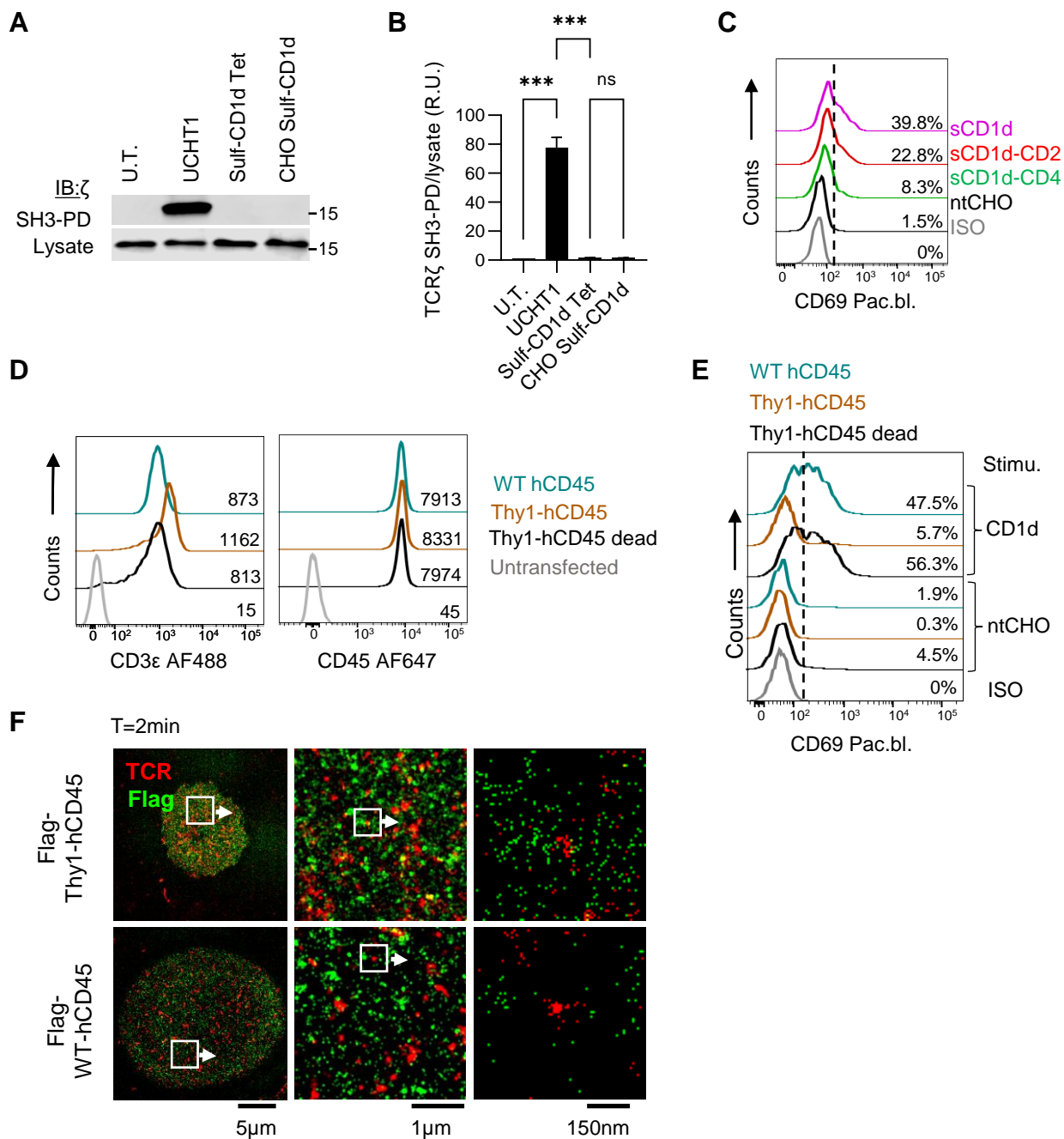


**Figure S9. Size-dependent DP10.7 TCR signaling in the absence of Nck-recruiting conformational change (Related to Figure 7, figure legend on following page).**



**Figure S9. Size-dependent DP10.7 TCR signaling in the absence of Nck-recruiting conformational change.**

**(A)** Detection of CD3 $\epsilon$  conformational change by Nck SH3.1 TCR pulldown in DP10.7 Jurkat T cells. Cells were incubated with anti-CD3 $\epsilon$  mAb UCHT1, sulfatide-loaded CD1d tetramer, or left untreated (U.T.), and blotted for TCR $\zeta$  in pulldowns and input lysates.

**(B)** Quantitation of blots as in **(A)**. Data are presented as normalized ratios of TCR $\zeta$  density in Nck SH3.1 pulldown lanes (TCR $\zeta$  SH3-PD) over TCR $\zeta$  density in corresponding input lysates. R.U., relative units.  $n = 3$ , data are mean  $\pm$  SD.

**(C)** Representative histogram cascade plot of surface CD69 expression levels of DP10.7 Jurkat T cells corresponding to **Figure 7F**. Numbers denote % CD69<sup>+</sup> cells determined by isotype antibody labeling of resting DP10.7 Jurkat T cells (demarcated by dashed line).

**(D)** Representative histogram cascade plot of surface staining of endogenous TCR and CD45 in DP10.7 Jurkat T cell transductants expressing the indicated CD45 chimeras. Numbers represent MFI.

**(E)** Representative histogram cascade plot of surface CD69 expression levels of DP10.7 Jurkat T cell transductants, incubated with sulfatide-loaded CD1d-CHO cells, corresponding to Figure 7L. Due to variability in CD69 levels in resting DP10.7 Jurkat T cell transductants, change in % CD69<sup>+</sup> DP10.7 cells was calculated for Figure 7L ( $\Delta\%$ CD69<sup>+</sup>).

**(F)** Representative dSTORM images of TCR and Flag-tag localizations at synapses of DP10.7 Jurkat T cells transduced with the indicated Flag-tagged CD45 chimeras.

**Supplementary Table 1. Quantitation of cell surface molecules**

Cell Type	Construct expressed	mol/ $\mu\text{m}^2$	% of endogenous CD45/CD148
G8 T cell hybridoma (G8 <sub>H</sub> )	None (Endogenous CD45)	793.8	100
	Thy-CD45	3.6	0.5
	Thy1-CD45*	2.9	0.4
	CD43-CD45	16.3	2.1
	None (Endogenous CD148)	43.8	100
	2FN3-CD148	19.4	44.3
	2FN3-CD148*	18.8	42.3
	WT-CD148	3.2	7.3
Primary G8 T cells (G8 <sub>P</sub> )	None (Endogenous)	47.3	100
DP10.7 Jurkat T cell	None (Endogenous CD45)	622	100
	Thy-CD45	34.1	5.3
	Thy1-CD45*	72.2	11.2
	WT-CD45	38.0	5.9

\*Catalytically inactive mutant

**Extended Data Table 2. Oligonucleotide sequences**

T22 constructs	T22	Forward: tcgggtggcggcggtctgggtcacactcgcttaggtatttc
		Reverse: gaggaagcttcagtcagggtgacagtaaagactcg
	$\beta$ -2M	Forward: gatatctcgagtcgcttcagtcgtcagcatgg
		Reverse: ccagagccgccacccgagccgcctccgccgaaccgcca cctcccatgtctcgatcccagtagac
	BamHI site insertion	Forward: taatggatcctgcatggaaagtgggtgc
		Reverse: taatggatcctcagtcggcagaacctg
	BamHI site removal	Single primer: gatgggaggatccgtggatttgattgttg
	CD45 STOP insertion	Forward: gagcaagggcgagtagctgttcaccgg
		Reverse: ccggtgaacagctactcgcccttgctc
RT-PCR	T22-SCD	Forward: atggctcgtcggtgacc
		Reverse: aggtgacagtaaagactcgcca
	Flag-mouseCD45	Forward: gattacaaggatgacgacgataagccta
		Reverse: cgtgaactctgggttgagct
	Flag-mouseCD148	Forward: gattacaaggatgacgacgataagccta
		Reverse: gatgtaaccattagtcttccaacatgct
	CD1d-SCD	Forward: ggggggatcccggtactcgagggttcaataag
		Reverse: agtcgcggccgctcacaggacgccctgatagga
	Flag-humanCD45	Forward: gggattataaggacgatgatgacaaaca
		Reverse: tgaaccttgatttaaagctggacttg
	Mouse $\beta$ -actin	Forward: ctgtccctgtatgcctctg
		Reverse: atgtcacgcacgatttcc
	Hamster $\beta$ -actin	Forward: ctgtccctgtatgcctctg
		Reverse: atgtcacgcacaatttcc
	Human $\beta$ -actin	Forward: gagcacagagcctcgcttt
		Reverse: ccaggaaggaaggctggaag